Solar Updraft Tower

Research Physics Final Project

Noam Segal, wsegalnoam@gmail.com.

Noam Nov Kolodny, naominovkolodny@gmail.com.

Supervisor: Dr. Eduard Moses

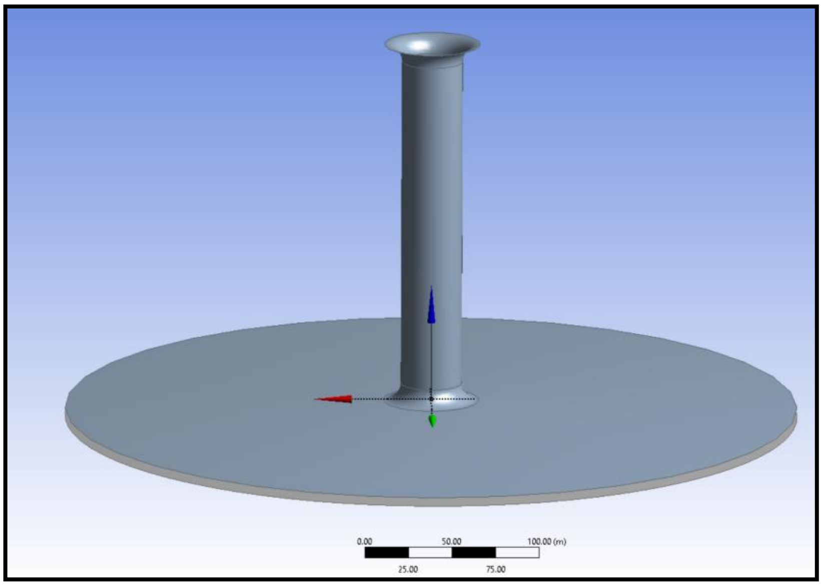

Table of Contents

List of Figures

List of Tables

Executive summary

1. We made a simplified calculation of a Solar Updraft Tower.
2. We, then, built an accurate simulation of a Solar Updraft Tower Power Plant, using the commercial CFD code Star-CCM+ from Siemens.
3. We performed a parametric study to investigate the influence of 2 design parameters on the operation of an Energy Tower.
4. Our CFD calculations show that the power output of this device is unexpectedly (by comparison to our initial estimations) small, making the device economically non-viable.

1. Motivation

Energy is the keystone of all life on earth, the primary source of which is the sun. History has taught us that the more we learn to obtain and use this energy, the more human development is enabled and accelerated. But clean, efficient, and cheap energy production is still being worked on. As of today, energy production all around the globe often falls short of local requirements, which results in frequent power outages. As the world economy and population continue to rise, energy consumption is expected to go up with them. Fossil fuel is limited and damaging to the environment and the humans within it, hence the utmost importance of alternative energy sources, especially solar, in meeting rising energy demands. Use of solar energy may also aid in solving a very big threat to human health - pollution. Environmental pollution occurs when pollutants contaminate the natural surroundings. Pollution disrupts the fine balance of our ecosystem, affects our normal day-to-day lifestyles, and shortens our health spans. Pollution is now peaking due to the development and modernization of many once rural areas. Contemporaneous with the improvements in science and technology, there has been a massive change in human potential. Entrapped by our own industrial and technological developments, air pollution threatens us on a personal daily basis - and is one of the most dangerous forms of pollution. A biological, chemical, and physical alteration of the air occurs when smoke, dust, and any harmful gases and particles are introduced into the atmosphere and make it difficult for all living beings to survive as their concentration increases and the air becomes more contaminated. Burning of fossil fuels, for agriculture related activities, mining operations, exhaust from industries and factories, and household cleaning products entails air pollution. People release a huge number of chemical substances into the air every day. The effects of air pollution are alarming. It causes global warming, acid rains, respiratory and heart problems, and eutrophication. A lot of wildlife species are forced to change their habitat to survive. Soil pollution occurs when the presence of pollutants, contaminants, and toxic chemicals in the soil is in high concentration that has negative effect on wildlife, plants, humans, and ground water. Industrial activity, waste disposal, agricultural activities, acid rain, and accidental oil spill are the main causes of soil pollution. This type of contamination influence health of humans, affects the growth of plants, decreases soil fertility, and changes the soil structure. Water pollution can lead our world on a path of destruction. Water is one of the greatest natural resources for humans. Life as we know it cannot exist without water. The key causes of the water pollution are industrial waste, mining activities, sewage and wastewater, accidental oil leakage, marine dumping, chemical pesticides & fertilizers, burning of fossil fuels, animal waste, urban development, radioactive waste, and leakage from sewer lines. As a result, there is less water available for drinking, cooking, irrigating crops, and washing.

2. A large-scale solar energy production device – Solar Updraft Tower Power Plant

To eliminate many of the problems stated above, one solution can be a solar updraft tower, that can create energy without polluting its environment.

The general design of a solar updraft power consists of a large green house like body, which is dyed black to help the air heat efficiently, and a large chimney tower, with a wind turbine at the top of it. To start, the air inside the greenhouse like body is heated using direct sunlight. Then, the air begins to travel towards the middle of the tower, resulting in a hot air updraft towards the chimney. The airflow drives the wind turbines that are shrouded and therefore yield more power, that are placed at the very top of the chimney and produce electricity.

The solar updraft tower is unique since it can be operated with virtually no carbon footprint, fuel consumption, or waste production. It generates clean, cost effective and efficient electrical power without damaging effects. The tower can work year-round, in almost any weather conditions, assuming there is sunlight.

3. History

The first chimney turbine was depicted by Leonardo DaVinci as a smoke jack and was illustrated by him 500 years ago. A gored animal could be rotated vertically above a fire or in an oven in a similar manner to popular dishes such as Shawarma and Doner Kebab.

Beginning in 1975, Robert E. Lucier applied for patents on a solar chimney electric power generator; between 1978 and 1981 patents (since expired) were granted in Australia, Canada, Israel, and the US.

In 1926 Prof Engineer Bernard Dubos proposed to the French Academy of Sciences the construction of a Solar Aero-Electric Power Plant in North Africa with its solar chimney on the slope of a large mountain.

In 1982, a small-scale experimental model of a solar draft tower was built in Manzanares, Ciudad Real, 150 km south of Madrid, Spain. The power plant operated for approximately eight years. The tower's guywires were not protected against corrosion and failed due to rust and storm winds. The tower blew over and was decommissioned in 1989.

The solar tower was built of iron plating only 1.25 millimeters thick. The chimney had a height of 195 meters and a diameter of 10 meters with a collection area (greenhouse) of 46 hectares (110 acres) and a diameter of 244 meters (801 ft), obtaining a maximum power output of about 50 kW. Various materials were used for testing, such as single or double glazing or plastic (which turned out not to be durable enough). During its operation, 180 sensors measured inside and outside temperature, humidity and wind speed data was collected on a second-by-second basis.

In December 2010, a tower in Jinshawan in Inner Mongolia, China, started operation, producing 200 kilowatts.[9] The 1.38 billion RMB (USD 208 million) project was started in May 2009. It was intended to cover 277 hectares (680 acres) and produce 27.5 MW by 2013 but had to be scaled back. The solar chimney plant was expected to improve the climate by covering loose sand, restraining sandstorms. Critics have said that the $50[m]$ tall tower is too short to work properly and that it was a mistake to use glass in metal frames for the collector, as many of them cracked and shattered in the heat.

In mid-2008, the Namibian government approved a proposal for the construction of a 5400 MW solar chimney called the 'Greentower'. The tower is planned to be 1.5 kilometers (4,900 ft) tall and 280 meters (920 ft) in diameter, and the base will consist of a 37 square kilometers (14 sq mi) greenhouse in which cash crops can be grown.

In Xian, central China, a 60-metre urban chimney with a surrounding collector has significantly reduced urban air pollution. This demonstration project was led by Cao Junji, a chemist at the Chinese Academy of Sciences' Key Laboratory of Aerosol Chemistry and Physics.

4. Scope of the present work

In this work we present an ideal mathematical model of the flow and power production in a Solar Updraft Tower (SUT), to study the influence of various factors such as height and diameters on its operation and to optimize it.

The work is organized as follows:

1. We show an approximate method to estimate the power output of the tower.
2. Using this simple approach, we estimate the influence of the tower's various physical parameters on its power output.
3. We then present a more accurate CFD (Computational Fluid Dynamics) model of the tower and analyze features of the flow.
4. We will use this accurate model to investigate the influence of various geometric features of the tower on its output.
5. Finally, we summarize what has been shown, and draw conclusions.

5. Simplified mathematical model of a Solar Updraft Tower

In this section, we estimate the energetic output of the SUTPP. To achieve that, we calculate the pressure inside the tower and outside it and use Bernoulli's equation to calculate the flow velocity and the kinetic energy of the stream entering the wind turbines at the upper end of the tower.

Primarily, the two following things are shown:

1. The tower's power output is:

$$P_{out} = \frac{\pi}{4} \cdot \sqrt{2R_s \cdot T_H} \cdot p_0 \left[\left(1 - \frac{g}{c_p} \cdot \frac{h}{T_H}\right)^{\frac{k}{k-1}} - \left(1 - \frac{g}{c_p} \cdot \frac{h}{T_0}\right)^{\frac{k}{k-1}} \right]^{1.5} \cdot d^2 \qquad (1)$$

Where d and h are the tower's diameter and height accordingly, T_H and T_0 are the temperatures at the base of the tower and outside accordingly, $\frac{g}{c_p}$ is the atmospheric lapse-rate, k is the adiabatic index for air, p_0 is the atmospheric pressure, and R_s is the mass-specific gas constant of air.

2. The radius of the tower's heat absorbing base is given by:

$$R = \sqrt{\frac{P_{out}}{\pi \cdot Pd_{sun} \cdot Ap_{base}}} \qquad (2)$$

Where Pd_{sun} is the *Power Density* of the solar radiation, and Ap_{base} is the *Absorptive Power* of the black paint used.

5.1. Geometric Configuration

Consider an axisymmetric tower – *Fig. 1* of height h and diameter d whose lower base is emitting a heat flux Q_h (by means of a large solar energy capturing device of radius R consisting of ground surface painted in black and covered with transparent glass). Wind Turbines will be placed at the upper base of the tower to convert the kinetic energy of the flow into electric energy.

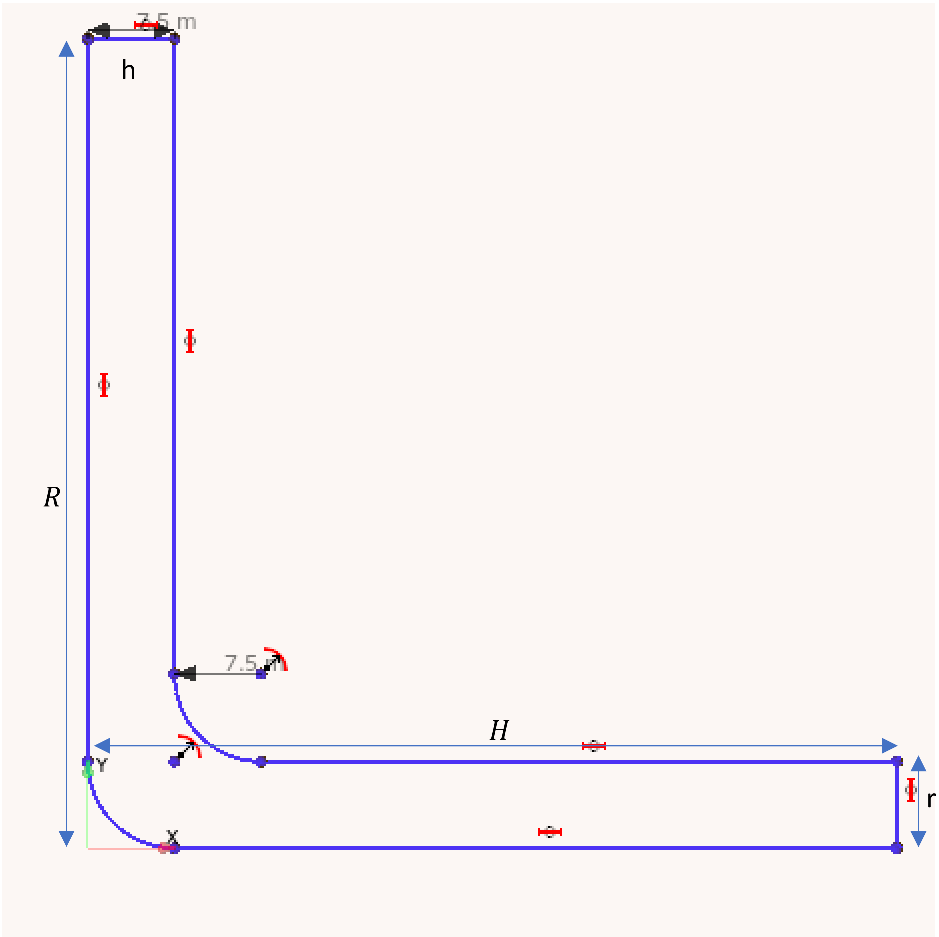

Fig. 1: Geometric configuration of the tower

5.2. Atmospheric pressure and temperature distribution

Temperature, pressure, and density are distributed along height in the free atmosphere according to what is called "adiabatic distribution".

5.2.1. Temperature distribution with height

The atmospheric adiabatic temperature distribution with height is linear, given by:

$$T = T_h - \frac{g}{c_p} \cdot z \tag{3}$$

Where the slope of the graph is called "atmospheric lapse rate":

$$\Gamma = \frac{g}{c_p} \left[\frac{K}{m}\right] \tag{4}$$

We observe that Γ is approximately 9.8 $[\frac{K}{km}]$.

5.2.2. Pressure distribution with height

The pressure as a function of height (z) given by the equation:

$$p = p_0 - \int_0^z \rho \cdot g \cdot dz \tag{5}$$

Accounting for the fact that the pressure, p, must also obey the ideal gas law, and accounting for (5) as well, we have:

$$p_0 - \int_0^z \rho \cdot g \cdot dz = \rho \cdot R_s \cdot T_h \cdot \left(1 - \frac{g}{c_p \cdot T_h} \cdot z\right) \tag{6}$$

Differentiating (6), we obtain:

$$-\rho \cdot g = R_s \cdot T_h \cdot (1 - \frac{g}{c_p \cdot T_h} \cdot z) \cdot \frac{\mathrm{d}\rho}{\mathrm{d}z} - \rho \cdot R_s \cdot \frac{g}{c_p} \tag{7}$$

Accounting for:

$$\begin{cases} c_p - c_v = R_s \\ \dfrac{c_p}{c_v} = k \end{cases} \tag{8}$$

Where k is the adiabatic index (1.4 for air which has a diatomic molecule) in (7) and regrouping the terms, we obtain:

$$-\frac{1}{k} \cdot \rho \cdot g = R_s \cdot T_h \cdot (1 - \frac{g}{c_p \cdot T_h} \cdot z) \tag{9}$$

We can re-write (9) as:

$$\frac{d\rho}{\rho} = -\frac{1}{k} \cdot \frac{g}{R_s \cdot T_h \cdot \left(1 - \frac{g}{c_p \cdot T_h} \cdot z\right)} \cdot dz \tag{10}$$

Integrating (10), we obtain:

$$\rho = \rho_h \cdot \left(1 - \frac{g}{c_p \cdot T_h} \cdot z\right)^{\frac{1}{k-1}} \tag{11}$$

Where index "h" signifies "Hot" - and is the density at ground level inside the tower. Using the ideal gas law and accounting for (1) and (9), we obtain the pressure distribution as:

$$p = \rho_h \cdot R_s \cdot T_h \cdot \left(1 - \frac{g}{c_p \cdot T_h} \cdot z\right)^{\frac{k}{k-1}} \tag{12}$$

Pressure and temperature distribution outside the tower can be obtained by (1) and (10) by simply substituting the index h for index 0, representing conditions on the ground outside the tower.

5.3. Pressure difference between inside and outside the tower at upper base

We will use the ideal gas law to determine the density inside the tower, assuming that the pressure is the atmospheric pressure at ground level.

$$\rho_h = \frac{p_0}{R_s \cdot T_h} \tag{13}$$

Where index h signifies inside the tower (Hot) and index 0 signifies in the free atmosphere outside the tower.

From the ideal gas law, we obtain:

$$\rho_0 = \frac{p_0}{R_s \cdot T_0} \tag{14}$$

Using (11), we obtain:

$$\rho_h = \frac{p_0}{R_s \cdot T_h} \tag{15}$$

Using (14) in (12) we obtain the outside pressure as:

$$p_{outside} = p_0 \cdot \left(1 - \frac{g}{c_p \cdot T_0} \cdot z\right)^{\frac{k}{k-1}} \tag{16}$$

Using (15) in (12) we obtain the inside pressure as:

$$p_{inside} = p_0 \cdot \left(1 - \frac{g}{c_p \cdot T_h} \cdot z\right)^{\frac{k}{k-1}} \tag{17}$$

From (14) and (15) we obtain the pressure difference at the top of the tower

as:

$$\Delta p = p_{inside} - p_{outside} \tag{18}$$

5.4. Flow rate from inside to outside the tower

Using Bernoulli's law, we have the flow velocity as:

$$v = \sqrt{\frac{\Delta p \cdot 2}{\rho}} \tag{19}$$

5.5. Power output

The gross power output or power output potential is given by:

$$P_{out} = \Delta p \cdot \dot{V} \tag{20}$$

Where $\dot{V}$ is the volumetric flow rate, given by:

$$\dot{V} = A \cdot v = \frac{\pi \cdot d^2}{4} \cdot v \tag{21}$$

We can continue to develop (20):

$$P_{out} = A \cdot v \cdot \Delta p = \frac{\pi d^2}{4} \cdot v \cdot \Delta p \tag{22}$$

We can substitute v and Δp, as they were previously derived:

$$P_{out} = \frac{\pi d^2}{4} \cdot \sqrt{\frac{\Delta p \cdot 2}{\rho_h}} \cdot \Delta p \tag{23}$$

$$P_{out} = \frac{\pi d^2}{4} \cdot \sqrt{\frac{2}{\rho_h}} \cdot \Delta p^{1.5} \tag{24}$$

$$P_{out} = \frac{\pi d^2}{4} \sqrt{\frac{2}{\rho_h}} \cdot \left[\left(\rho_H \cdot R_s \cdot T_h \left(1 - \frac{g}{c_p} \cdot \frac{h}{T_h}\right)^{\frac{k}{k-1}}\right) - \left(\rho_0 \cdot R_s \cdot T_0 \left(1 - \frac{g}{c_p} \cdot \frac{h}{T_0}\right)^{\frac{k}{k-1}}\right)\right]^{1.5} \tag{25}$$

Finally, we can write the power output as:

$$P_{out} = \frac{\pi}{4} \cdot \sqrt{2R_s \cdot T_h} \cdot p_0 \left[\left(1 - \frac{g}{c_p} \cdot \frac{h}{T_h}\right)^{\frac{k}{k-1}} - \left(1 - \frac{g}{c_p} \cdot \frac{h}{T_0}\right)^{\frac{k}{k-1}}\right]^{1.5} \cdot d^2 \ \blacksquare \tag{26}$$

5.6. Base Radius

Let us define:

$$Pd_{base} \equiv Pd_{sun} \cdot Ap_{base} \tag{27}$$

As the actual density of power input received by the tower.

Using a base surface area of:

$$S_{base} = \pi R^2 \tag{28}$$

We can calculate the power input P_{in} as:

$$P_{in} = Pd_{base} \cdot S_{base} = \pi \cdot Pd_{base} \cdot R^2 \tag{29}$$

And since we want a constant operating power output, we know that:

$$P_{out} = P_{in} \tag{30}$$

And so, we can isolate the radius R:

$$P_{out} = \pi \cdot Pd_{base} \cdot R^2 \tag{31}$$

$$R^2 = \frac{P_{out}}{\pi \cdot Pd_{base}} \tag{32}$$

$$R = \sqrt{\frac{P_{out}}{\pi \cdot Pd_{base}}} \;\blacksquare \tag{33}$$

5.7. Choosing Parameter Values

The relevant constants we will be using are:

- $k = 1.4$
- $\frac{g}{c_p} = 9.77 \times 10^{-3} \left[\frac{K}{m}\right]$
- $R_s = 287.05 \left[\frac{\mathrm{J}}{\mathrm{Kg} \cdot K}\right]$
- $p_0 = 101325[Pa]$

We will also assume the following numerical data:

- Height of the tower: $h = 1500[m]$
- Diameter of the tower: $d = 70[m]$
- Outside temperature: $20[°C] = 293[K]$
- Inside temperature: $60[°C] = 353[K]$
- Solar radiation power density: $Pd_{sun} = 1361 \left[\frac{W}{m^2}\right]$
- Base absorptive power: $Ap_{base} = 0.99$

Substituting the relevant parameters in (1) we obtain:

$$P = 756[MW] \tag{34}$$

And using (2), the towers base radius will accordingly be:

$$R = \sqrt{\frac{7.5 \times 10^8}{\pi \cdot 1361 \cdot 0.99}} = 422[m] \tag{35}$$

Of course, it is impossible to utilize all the power potential given in (19). We transform this power potential in electric power by means of a wind turbine.

The typical efficiency of a shrouded wind turbine is of the order of magnitude:

$$\eta = 30\% \tag{36}$$

Therefore, we have a power output of:

$$P_{electric} = P \cdot \eta = 227[MW] \tag{37}$$

Just for comparisons sake, the average power output one coal power unit at Hadera is $\sim 441[MW]$, so this device might be equivalent to a conventional power station, without the pollution and mining hazards of coal, as well as without any fuel costs since sun power is free.

6. Mathematical Optimization

Parameter optimization can be done solely based on the mathematical model presented in the previous chapter - and can also be accomplished experimentally using the more advanced CFD simulations. This section is concerned in the first method.

The parameters eligible for optimization are the physical dimension parameters:

- Chimney height
- Chimney diameter
- Base radius
- Various curve angles

First, we may want to know if there is any maximum chimney height, beyond which the power output will start to decrease.

6.1. Maximum Chimney Height

We have found that this height is given by:

$$h_{max} = \frac{T_H^{1-k} - T_0^{1-k}}{\left(T_H^{-k} - T_0^{-k}\right)\frac{g}{c_p}} \tag{38}$$

We can achieve this by deriving $P_{out}(h)$ and finding the maximum point.

$$\begin{aligned} \frac{\mathrm{d}}{\mathrm{d}h} P_{out}(h) = -1.5\frac{\pi}{4}\sqrt{2R_s \cdot T_H} \\ \cdot p_0 d^2 \frac{k}{k-1}\left[\left(1 - \frac{g}{c_p}\cdot\frac{h}{T_H}\right)^{\frac{k}{k-1}} - \left(1 - \frac{g}{c_p}\cdot\frac{h}{T_0}\right)^{\frac{k}{k-1}}\right]^{0.5} \\ \cdot\left[\frac{g}{c_p T_H}\left(1 - \frac{g}{c_p}\cdot\frac{h}{T_H}\right)^{\frac{1}{k-1}} - \frac{g}{c_p T_0}\left(1 - \frac{g}{c_p}\cdot\frac{h}{T_0}\right)^{\frac{1}{k-1}}\right] = 0 \end{aligned} \tag{39}$$

Now we can solve for h:

$$\left[\left(1 - \frac{g}{c_p}\frac{h}{T_H}\right)^{\frac{k}{k-1}} - \left(1 - \frac{g}{c_p}\frac{h}{T_0}\right)^{\frac{k}{k-1}}\right]^{0.5}\left[\frac{1}{T_H}\left(1 - \frac{g}{c_p}\frac{h}{T_H}\right)^{\frac{1}{k-1}} - \frac{1}{T_0}\left(1 - \frac{g}{c_p}\frac{h}{T_0}\right)^{\frac{1}{k-1}}\right] = 0 \tag{40}$$

This means that either:

$$\left[\left(1 - \frac{g}{c_p}\frac{h}{T_H}\right)^{\frac{k}{k-1}} - \left(1 - \frac{g}{c_p}\frac{h}{T_0}\right)^{\frac{k}{k-1}}\right]^{0.5} = 0 \tag{41}$$

Which yields $h = 0$. This is not an option since the geometry dictates that $h > 0$.

Or:

$$\left[\frac{1}{T_H}\left(1-\frac{g}{c_p}\frac{h}{T_H}\right)^{\frac{1}{k-1}} - \frac{1}{T_0}\left(1-\frac{g}{c_p}\frac{h}{T_0}\right)^{\frac{1}{k-1}}\right] = 0 \quad (42)$$

$$\frac{1}{T_H}\left(1-\frac{g}{c_p}\frac{h}{T_H}\right)^{\frac{1}{k-1}} = \frac{1}{T_0}\left(1-\frac{g}{c_p}\frac{h}{T_0}\right)^{\frac{1}{k-1}} \quad (43)$$

$$T_H^{1-k}\left(1-\frac{g}{c_p}\frac{h}{T_H}\right) = T_0^{1-k}\left(1-\frac{g}{c_p}\frac{h}{T_0}\right) \quad (44)$$

$$\left(\frac{T_H^{1-k}}{T_H} - \frac{T_0^{1-k}}{T_0}\right)\frac{g}{c_p}\cdot h = T_H^{1-k} - T_0^{1-k} \quad (45)$$

$$\left(T_H^{-k} - T_0^{-k}\right)\frac{g}{c_p}\cdot h = T_H^{1-k} - T_0^{1-k} \quad (46)$$

So, the height h that gives the maximal power output is:

$$h_{max} = \frac{T_H^{1-k} - T_0^{1-k}}{\left(T_H^{-k} - T_0^{-k}\right)\frac{g}{c_p}} \;\blacksquare \quad (47)$$

For any realistic parameters we may choose - the following tower height h_{max} is too large for practical use. But it is good to be assured that for any value we pick later, we can't choose a *smaller* tower height which will give a higher power output.

The same goes for the chimney diameter and the base radius, because the wider they are the higher the power output will be.

6.2. Visualizing the Equations

Using the tower height h and the temperature inside the base of the tower (as a proxy for the heating zone's radius) as variables, we can plot a heatmap presenting the estimated power output as a function of these variables. Using a high range of values, a maximum power output can be seen for the tower height, with a continuing increase of power output as a function of the temperature – this can be observed in *Fig. 2*.

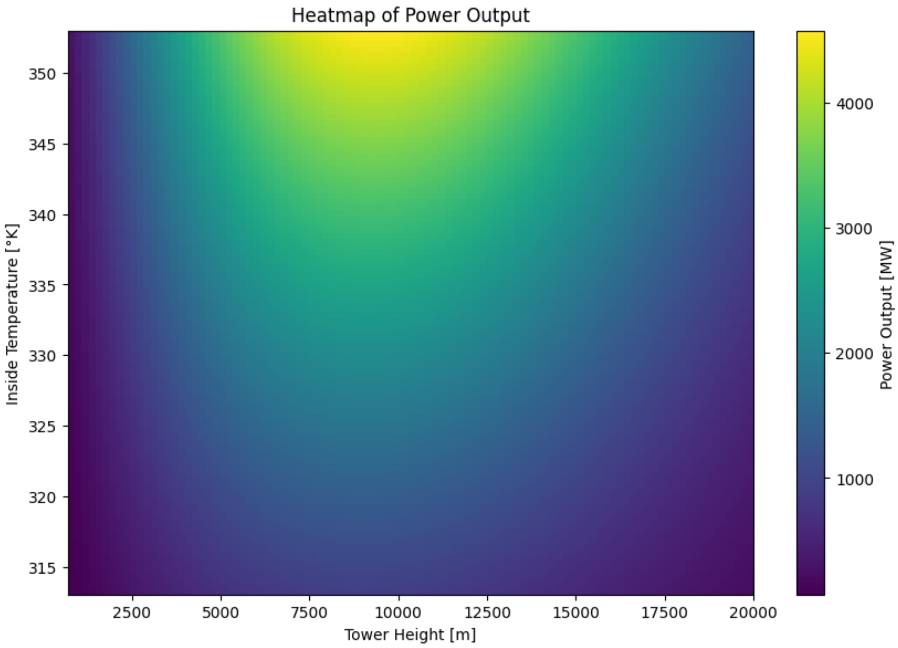

Fig. 2 Heatmap showing maximum tower height

Since the actual parameter values used will be far more limited, we can plot a heatmap that will represent the decision space more accurately – *Fig. 3*.

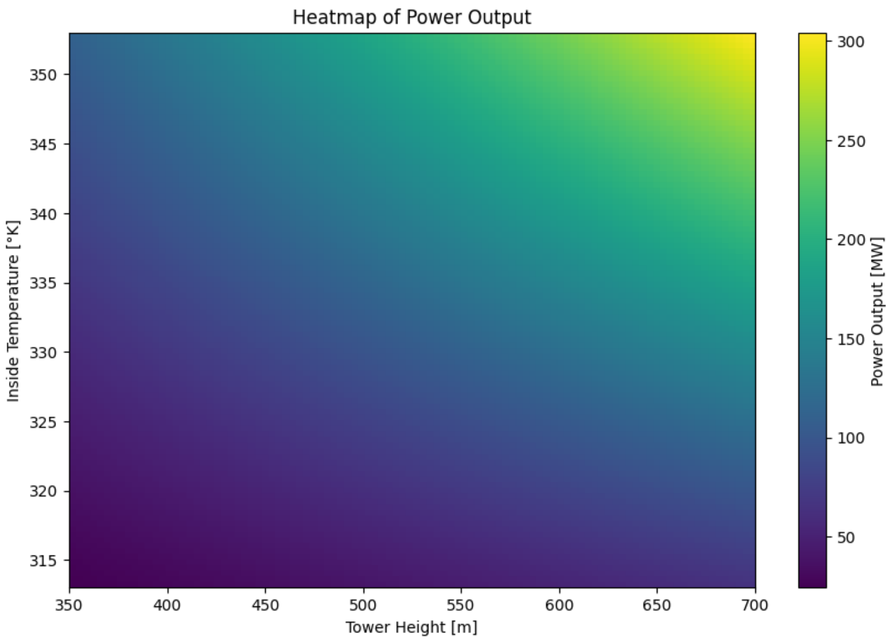

Fig. 3 Heatmap of power output with realistic values

From this we observe that unless the temperature is high (assuming an outside temperature of $20°C$, or equivalently $293°K$), the power output is quite minimal, that is, an order of magnitude lower. This raises the concern that unless a sufficiently high temperature can be maintained for an extended period, that the Solar Updraft Tower will perform poorly.

7. Accurate model of fluid flow

In this section we simulate a Solar Updraft Tower and monitor its various output parameters such as flow velocity, temperature gradient, and power output, as well as trying to optimize them.

To accurately model the SUT, the primary equations describing the fluid flow inside the tower need to be solved. These primary equations of the fluid flow are the basic laws of conservation applied everywhere in the physical world:

1. Conservation of mass (equation of continuity for fluid flows)
2. Conservation of momentum (Navier-Stokes equations for fluid flows)
3. Conservation of energy (energy equation)

7.1. Conservation of mass (Continuity equation)

The equation for conservation of mass, or continuity equation, can be written as:

$$\frac{\partial \rho}{\partial t} + \frac{\partial}{\partial x_i}(\rho u_i) = S_m \tag{48}$$

(48) is the general form of the mass conservation equation and is valid for incompressible as well as compressible flows.

7.2. Conservation of momentum (Navier-Stokes)

Conservation of momentum in the i direction in an inertial (non-accelerating) reference frame is described by:

$$\frac{\partial}{\partial t}(\rho u_i) + \frac{\partial}{\partial x_j}(\rho u_i u_j) = -\frac{\partial p}{\partial x_i} + \frac{\partial \tau_{ij}}{\partial x_j} + \rho g_i \tag{49}$$

where p is the static pressure and τ_{ij} is the stress tensor (described below). And ρg_i represents the gravitational body force in the i direction.

The stress tensor τ_{ij} is given by:

$$\tau_{ij} = \left[\mu\left(\frac{\partial u_i}{\partial x_j} + \frac{\partial u_j}{\partial x_i}\right)\right] - \frac{2}{3}\mu\frac{\partial u_l}{\partial x_l}\delta_{ij} \tag{50}$$

where μ is the molecular viscosity and the second term on the right-hand side is the effect of volume dilation.

7.3. Turbulence

The momentum equation ((49)) needs to be "closed" with a turbulence model (a way to specify the components of the stress tensor after Reynolds averaging the original equation).

Turbulence is modeled by the standard $k - \epsilon$ two equations model proposed by Jones and Launder. This model is very robust and has been successfully applied in a large variety of practical situations for many years. The model consists of transport equations for the turbulent kinetic energy (k) and its rate of dissipation (ϵ).

The transport equation for k is derived from the exact equation, while the one for ϵ has been derived using physical reasoning and is semi-empirical (see (51)).

$$\begin{cases} \rho \dfrac{Dk}{Dt} = \dfrac{\partial}{\partial x_i}\left[\left(\mu + \dfrac{\mu_t}{\sigma_k}\right)\dfrac{\partial k}{\partial x_i}\right] + G_k + G_b - \rho_\epsilon - Y_M \\ \rho \dfrac{D\epsilon}{Dt} = \dfrac{\partial}{\partial x_i}\left[\left(\mu + \dfrac{\mu_t}{\sigma_\epsilon}\right)\dfrac{\partial \epsilon}{\partial x_i}\right] + C_{1\epsilon}\dfrac{\epsilon}{k}(G_k + C_{3\epsilon}G_b) - C_{2\epsilon}\rho\dfrac{\epsilon^2}{k} \end{cases} \quad (51)$$

In the above equations, G_k represents the generation of turbulent kinetic energy due to the mean velocity gradients. G_b is the generation of turbulent kinetic energy due to buoyancy. Y_M represents the contribution of the fluctuating dilatation in compressible turbulence to the overall dissipation rate. C_1, C_2 and C_3 are constants. σ_k and σ_ϵ are the turbulent Prandtl numbers for k and ϵ respectively.

The eddy turbulent viscosity, μ_t, is computed by combining k and ϵ as follows:

$$\mu_t = \rho C_p \frac{k^2}{\epsilon} \quad (52)$$

The model constants in (51) have the following values:

$$C_{1\epsilon} = 1.44, \qquad C_{2\epsilon} = 1.92, \qquad C_\mu = 0.09, \qquad \sigma_k = 1, \qquad \sigma_\epsilon = 1.3 \quad (53)$$

7.4. Energy equation

The total enthalpy form of the energy equation is:

$$\frac{\partial}{\partial t}(\rho H)+\frac{\partial}{\partial x_i}(\rho u_i H)=\frac{\partial}{\partial x_i}\left(\frac{k_t}{c_p}\frac{\partial H}{\partial x_i}\right)+\tau_{ik}\frac{\partial u_i}{\partial x_k}+S_h \tag{54}$$

Assuming that the Lewis number, $Le\ = 1$, the conduction and species diffusion terms combine to give the first term on the right-hand side of (54), while the contribution from viscous dissipation appears (in the non-conservative form) as the second term. The total enthalpy, H, is defined as:

$$H=\sum j' m_{j'} H_{j'} \tag{55}$$

Where $m_{j'}$ is the mass fraction of species j' and

$$H_{j'}=\int_{T_{ref,j'}}^{T} c_{pj'}dT+h_{j'}^{o}\left(T_{ref,j'}\right) \tag{56}$$

Where $h_{j'}^{o}\left(T_{ref,j'}\right)$ is the formation enthalpy of species j' at the reference temperature $T_{ref,j'}$. (54) automatically includes pressure work and kinetic energy terms by the definition of the enthalpy ((56)), even though they are relatively small and could be safely neglected. (54) also includes the effect of enthalpy transport due to diffusion of species,

$$\frac{\partial}{\partial x_i}\sum j' h_{j'} J_{j'} \tag{57}$$

not in an explicit way but rather implicitly (as it is included in the first term on the right-hand side).

Observe that (54) does not include the term $\rho\vec{g}\cdot\vec{v}$. This term is non-negligible only for large geometric scales, which is the case here. Therefore, it will be added as a user-defined function to the energy equation.

8. Computational Fluid Dynamics Analysis

CFD analysis is a process whereby the above equations are solved numerically using the finite volume or the finite element method, under specified boundary conditions.

The solution is usually performed using one of the commercial CFD codes available.

The process of solving the problem involves the following steps:

1. Deciding the extent and nature of the computational domain and building the geometry describing it. This is usually done using a CAD (Computer Aided Design) tool. Star-CCM+ has one such tool embedded in it – 3D-CAD.
2. Meshing the computational domain, i.e., dividing it in finite volumes. After this division is achieved, the code will use *Galerkin* principle to convert the partial differential equations in non-linear algebraic equations on each of the finite volumes.
3. Prescribing the boundary conditions at the extremities of the computational domain.
4. Choosing the models to use in the simulation (e.g., the turbulence model) as well as the type of numerical solvers and the constitutive equation of the working fluid (in our case – ideal gas).
5. Prescribing an initial guess of the solution and solving the problem.
6. Finally, analyzing the results (which is called post-Processing), i.e., performing filled contours plots of various physical variables.

8.1. Geometry

Due to limitations in our available computational power, we could not solve the full three-dimensional flow in a reasonable amount of time. Therefore, we decided to neglect the effect of asymmetrical weather conditions, such as wind, on the operation of the SUT. In the absence of wind, the device is axisymmetric, and a two-dimensional axisymmetric solution can be utilized.

The layout of the SUT is outlined in *Fig. 1*. In Star-CCM+, when solving an axisymmetric problem, the symmetry axis must be the X axis. Therefore, the geometry lies on its side and the gravity acceleration is in the negative X direction.

8.1.1. Base case

We chose the base case to use the following dimensions:

- $H = 700\ [m]$
- $R = 700\ [m]$
- $r = 70\ [m]$
- $h = 75\ [m]$

The heat flux emitted by the ground is assumed to be $800\left[\frac{W}{m^2}\right]$.

8.2. Meshing

The mesh consists of $\sim 163{,}000$ elements, which are quadrilateral - *Fig. 4*. There are three types of possible mesh in two dimensions: triangular, quadrilateral, and polyhedral. We chose quadrilateral mesh because the elements have $90°$ angles (most of them) and thus ensure minimum numerical diffusion and maximum accuracy.

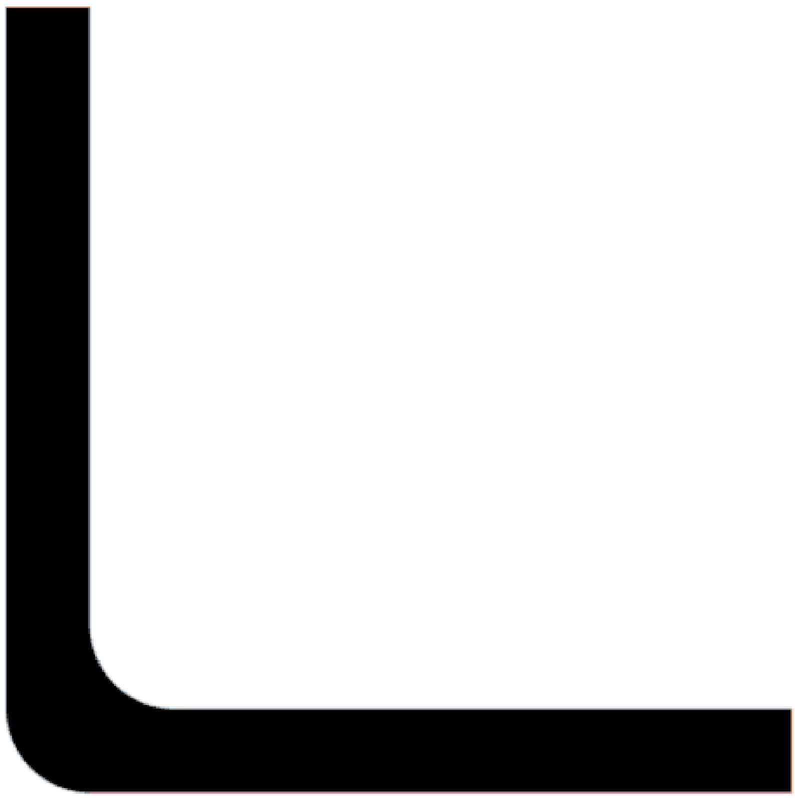

Fig. 4: Layout of the mesh

Near the walls of the tower, care was taken to refine the mesh (inflation layer) to properly capture the boundary layer of the flow. This can be seen in *Fig. 5*.

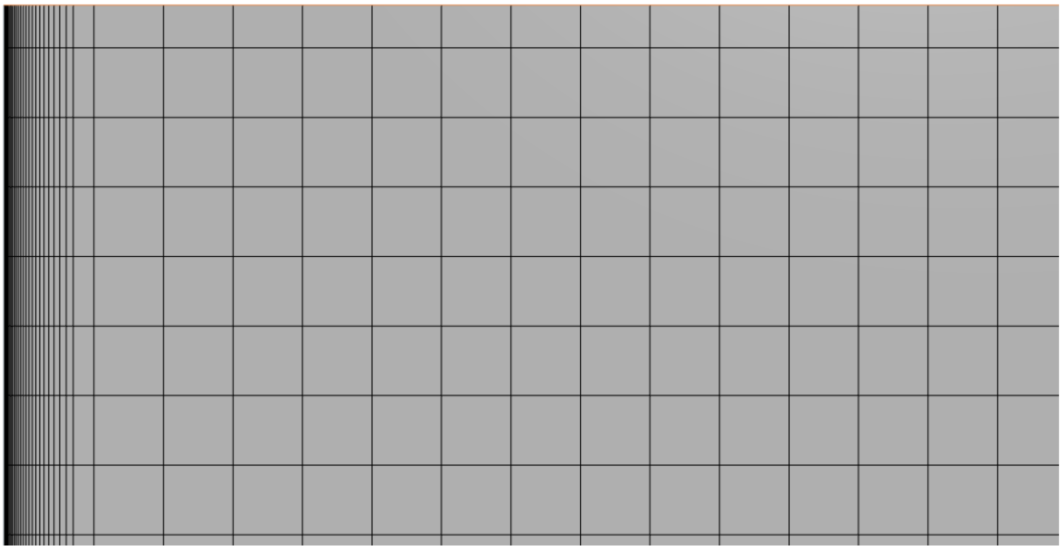

Fig. 5: Detail view showing the inflation layer on the wall.

We also took care to make an inflation layer on the axis of the geometry. This is not the usual procedure, but, specifically in our case, we expect the flow to be concentrated along the axis, and, therefore, we need to provide appropriate resolution to capture the velocity of the flow – Fig. *6*.

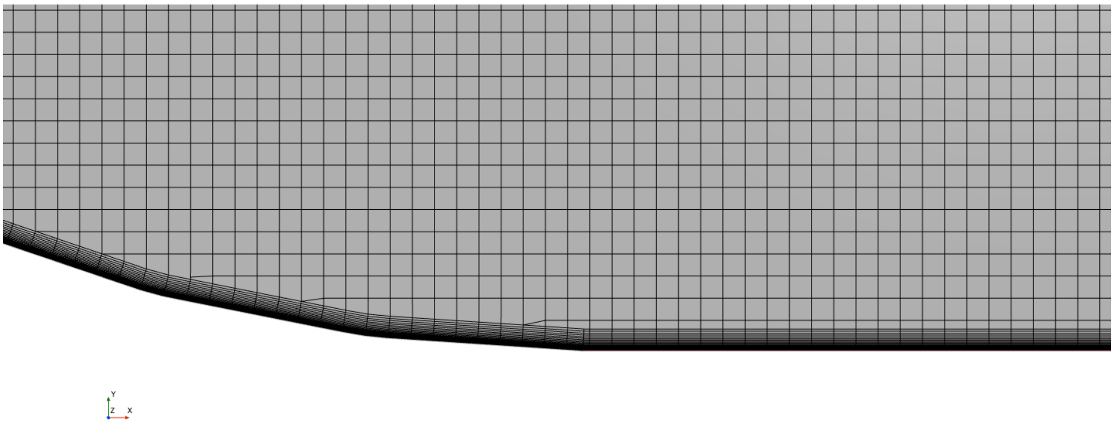

Fig. 6: Detail view showing the inflation layer on the axis.

8.3. Boundary Conditions

We must prescribe boundary conditions on the lower and upper atmospheric boundaries – see *Fig. 9*.

We will assume an adiabatic atmosphere on those boundaries and the conditions are described by equations written above:

1. Velocity: (19)
2. Temperature: (*3*)
3. Pressure: (16)

8.4. Physical Models

The flow equations can be solved using a coupled solver or a segregated solver.

A coupled solver forms coupled equations to solve pressure and velocity and includes all the couplings between the unknowns at once. This is appropriate if there are extreme physical conditions – since it requires more resources, but the result will be more accurate. On the other hand, a segregated solver does not solve for all the unknowns simultaneously. Instead, it divides the problem into segregated subproblems, and therefor requires less memory. This is more suitable for less extreme cases.

For these reasons we chose to work with a segregated flow solver, which requires less computer resources in comparison to a coupled solver, and the constitutive equation used is the ideal gas law.

After solving the flow equations, the power output is calculated using (1).

8.5. Initial Guess

The initial guess of the solution was calculated from the boundary conditions specified above – 8.3.

Fig. 7 presents the initial guess for temperature.

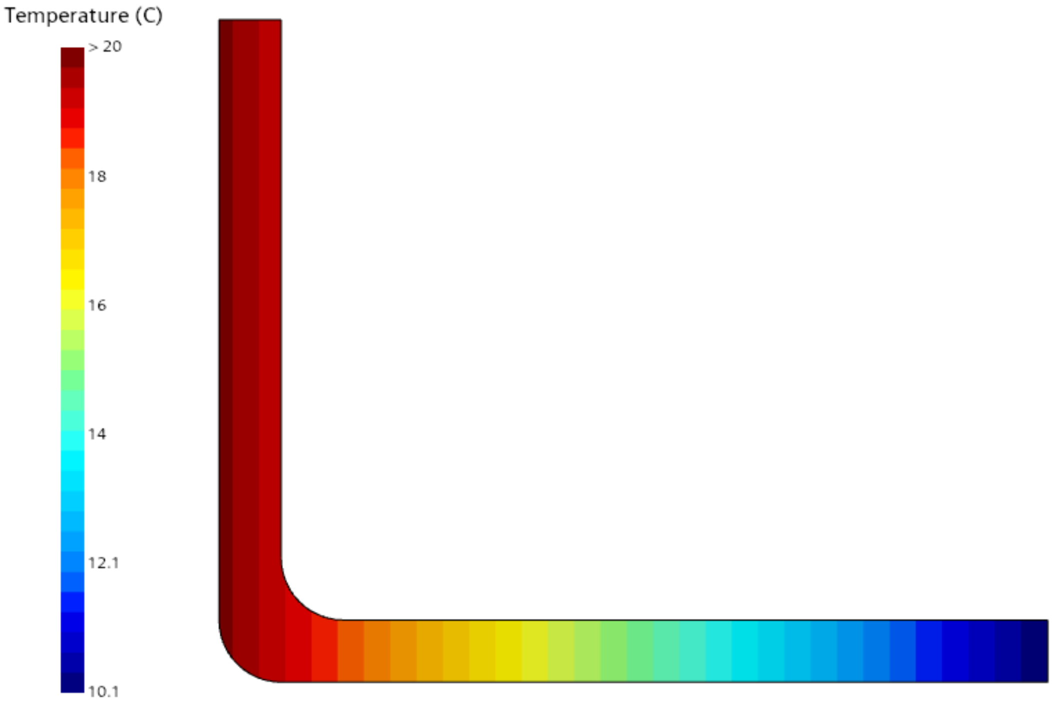

Fig. 7: Initial guess for temperature

Fig. 8 highlights the initial guess for pressure.

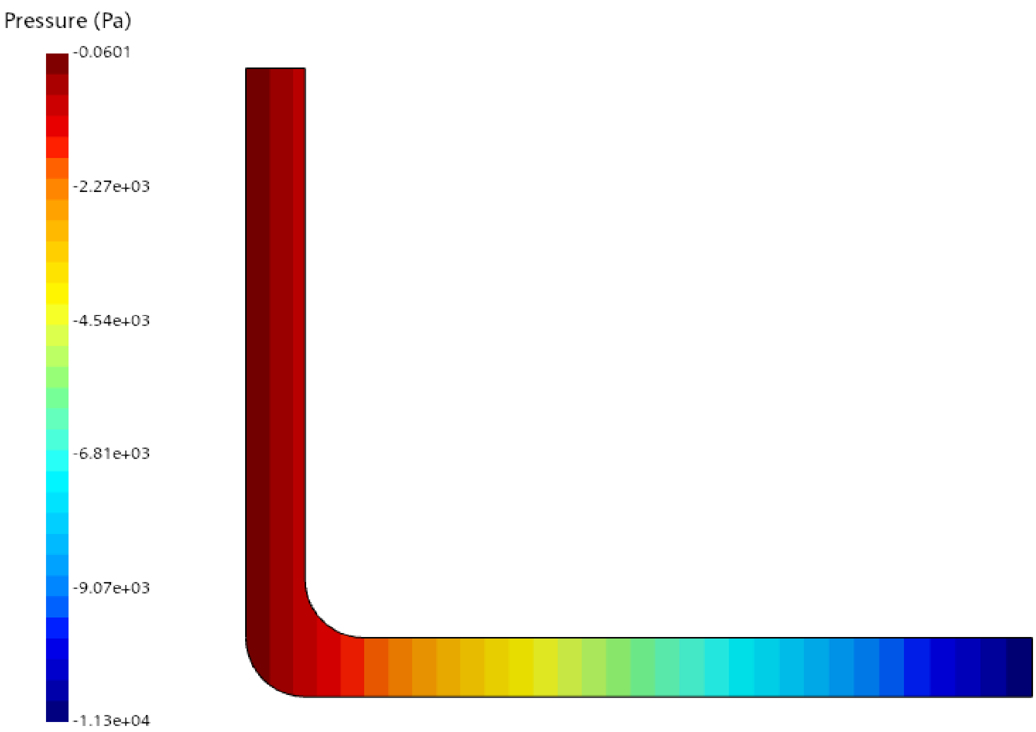

Fig. 8: Initial guess for pressure

8.6. Solving for Base Case

Here we computationally analyze the SUT device, using the basic parameters described in8.1.1, and examine features of the flow.

8.6.1. Velocity

Fig. 9 shows the velocity field for the base case. We observe the velocity to be mainly concentrated along the axis (as we assumed from the beginning). Also from the figure, we observe that the velocity increases as the air column ascends in the tower, prompting us to think that increasing the tower height will also increase the power output.

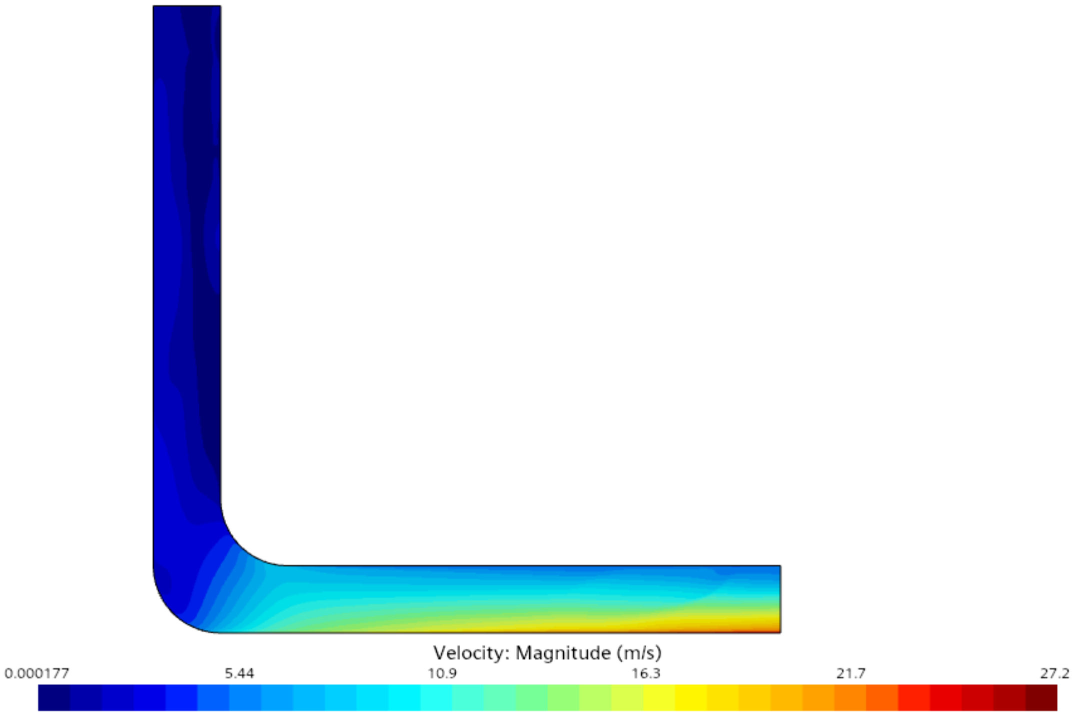

Fig. 9: Velocity field – base case.

8.6.2. Pressure

Fig. 10 Highlights the pressure field in the tower. We observe that the pressure is layered (because of the gravity). We also observe that the pressure gradient is slightly smaller towards the upper end of the tower, on account of the higher velocity.

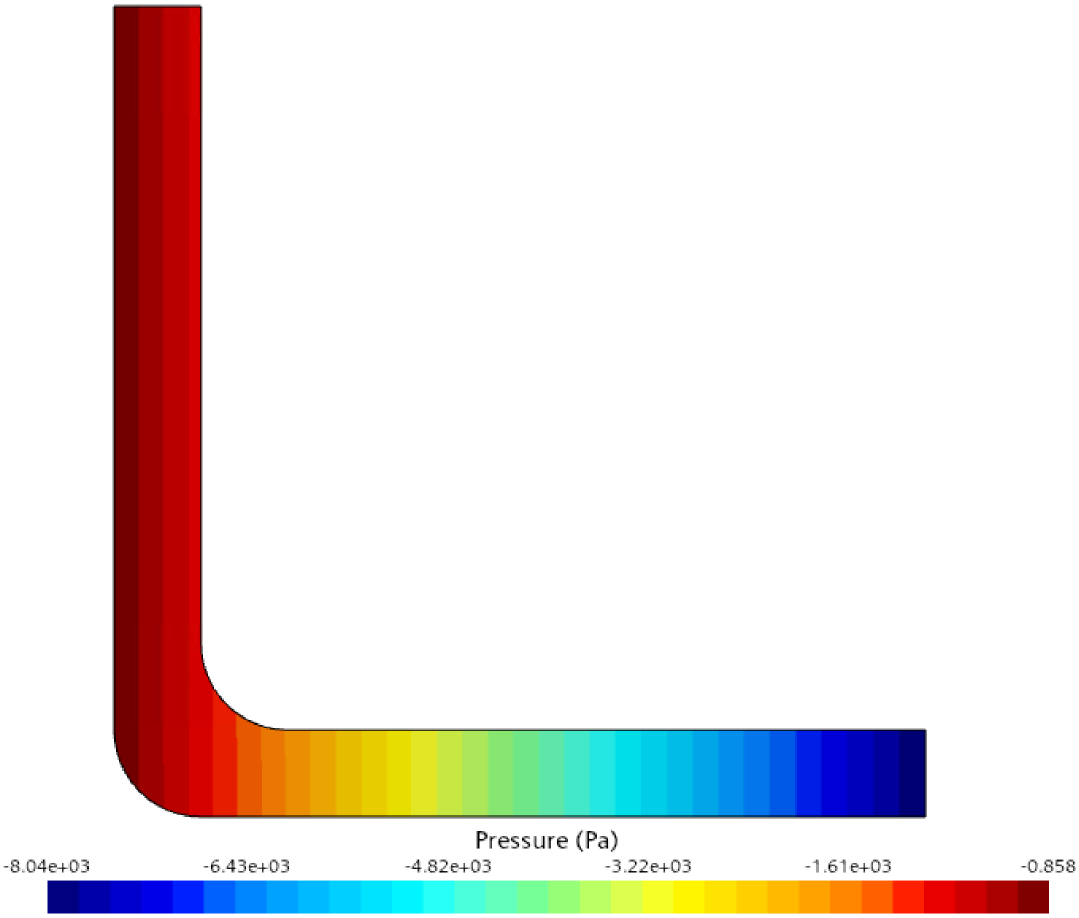

Fig. 10: Pressure field – base case.

8.6.3. Temperature

Fig. 11 presents the temperature field in the tower. We observe temperature to increase as the flow progresses in the base of the tower towards the axis. When the air flows upwards in the tower, the temperature decreases, as thermal energy turns into kinetic energy and propels the flow.

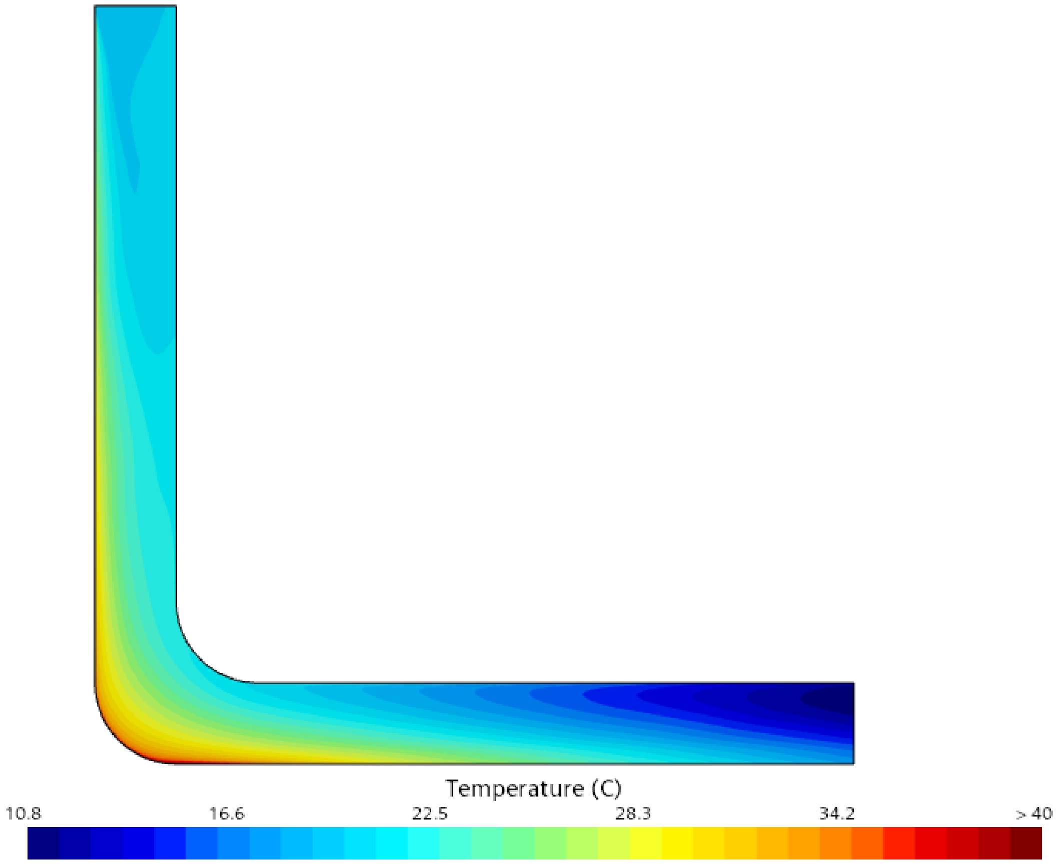

Fig. 11: Temperature field – base case.

8.7. Convergence

The integration of the equations must be continued until the calculated power output (taken here as a convergence monitor) stabilizes (i.e., its graph becomes a horizontal line) - *Fig. 12*.

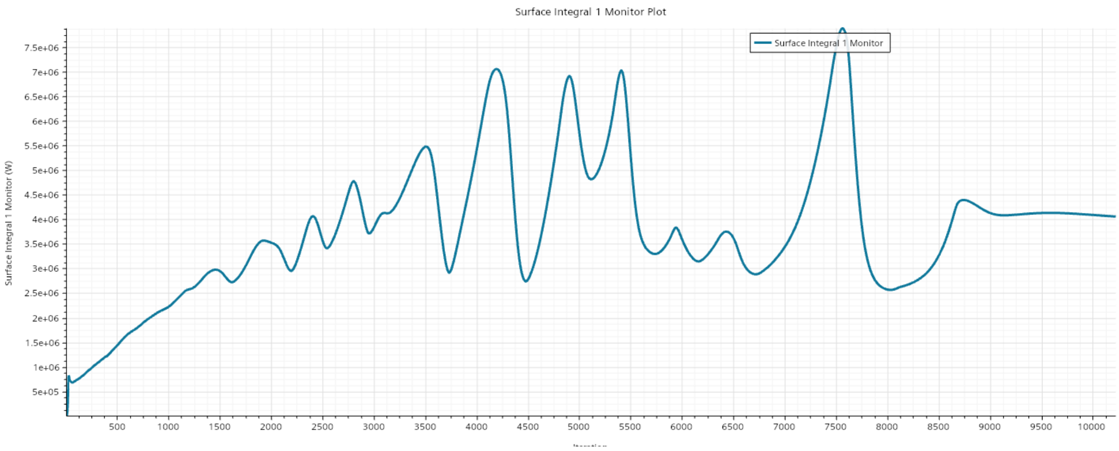

Fig. 12: Power output convergence graph.

9. Parametric Study

We performed a parametric study to highlight the influence of 2 parameters on the operation of the Energy Tower:

1. Tower height
2. Heating zone diameter

9.1. Tower height influence

We took the height of the tower to be radius of the heating zone to be $700[m]$ and varied the height of the tower from $500[m]$ to $1000[m]$.

The results of this parametric study are presented in

Table 1 and *Fig. 13*

Tower height [m]	Power Output [W]
500	3.52E+06
600	3.89E+06
700	4.06E+06
800	3.98E+06
900	3.64E+06
1000	3.29E+06

Table 1: Influence of tower height

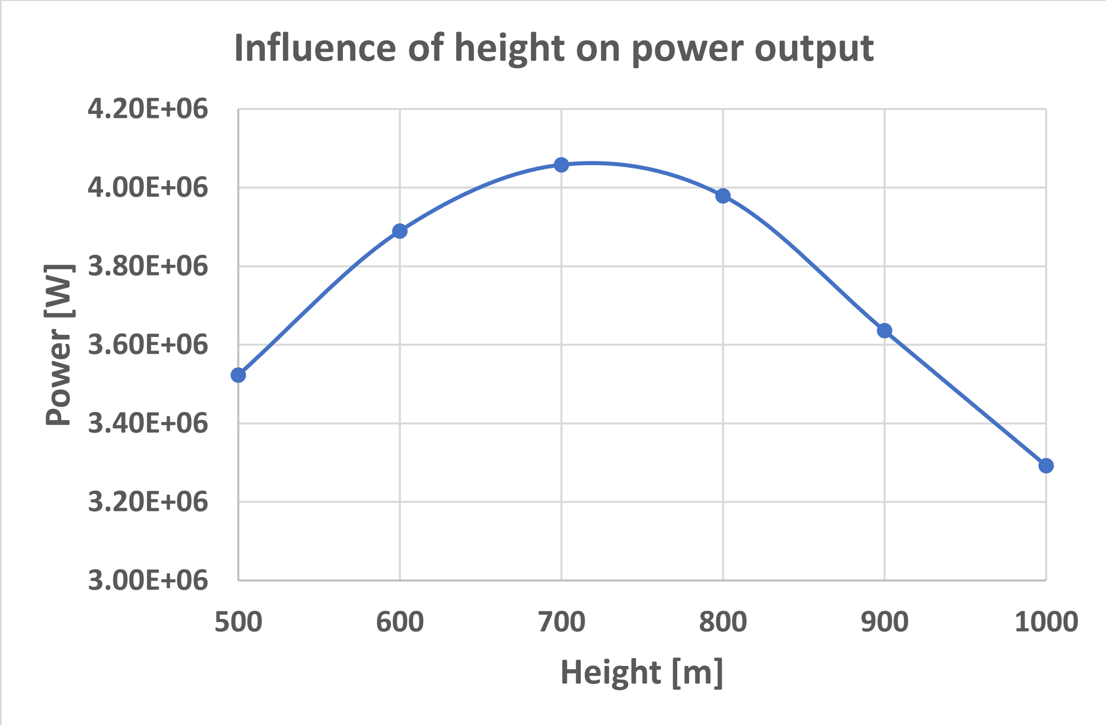

Fig. 13: Power output as a function of height.

In *Fig. 13* we observe that there is an optimum height for the specified radius of the heating zone ($700[m]$). The power output increases with the height of the tower up to $700[m]$ and then decreases. This can be explained by the friction with the tower walls, which increases linearly with the tower height, eventually overcoming the influence of the added buoyancy granted by increased height.

9.2. Radius of heating zone influence

We varied the radius of the heating zone from 700 m to 1000 m for two heights: 700 m and 1000m. Results are presented in

Table 2 and *Fig. 12*.

Radius [m]\Height [m]	700	1000
700	4.06E+06	3.29E+06
800	5.52E+06	5.02E+06
900	7.45E+06	7.24E+06
1000	9.61E+06	9.70E+06

Table 2: Influence of heating zone radius for two heights

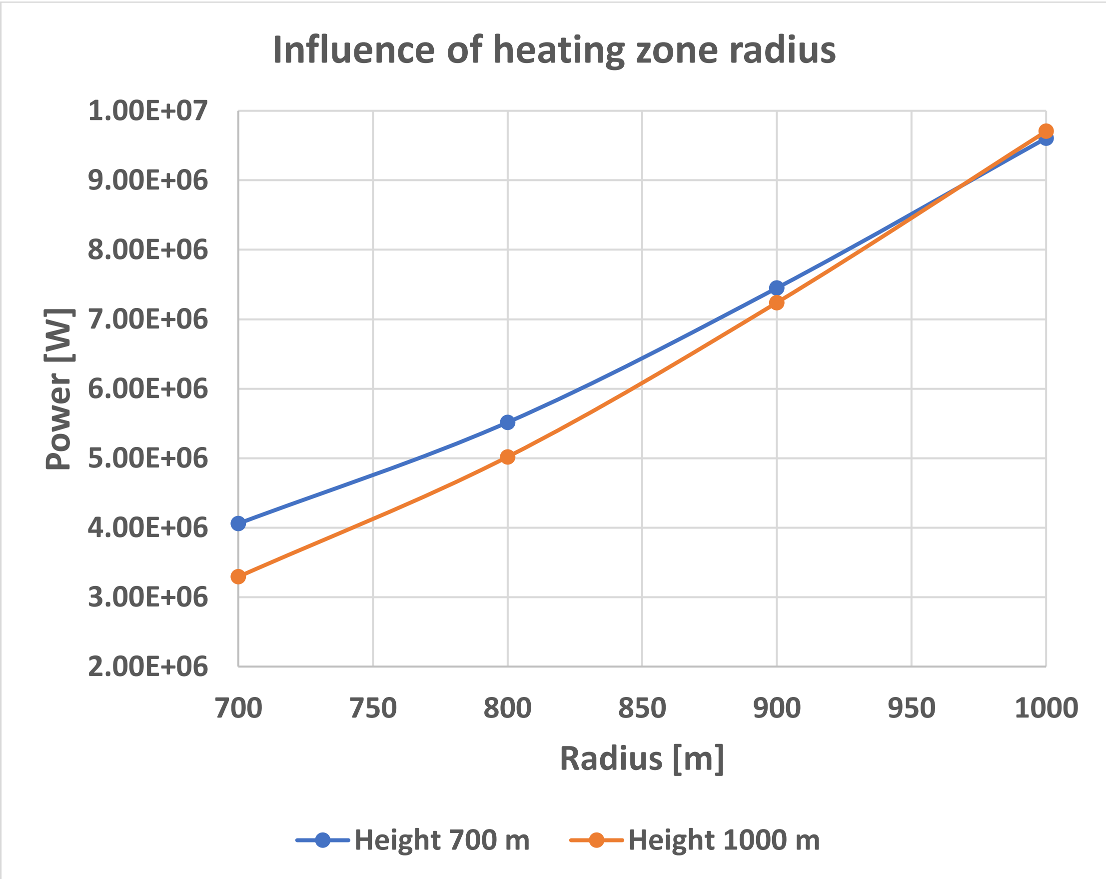

Fig. 14: Power output as a function of heating zone radius.

From *Fig. 12* we observe that, irrespective of the tower height, the power output increases almost parabolically with the radius of the heating zone. This is easily explained by the fact that the heating energy is proportional to the area of the ground within the heating zone, which, in turn, is proportional to the square of the radius.

We observe that the power output increases more dramatically with the heating zone radius when the tower has a height of $1000[m]$ than for $700[m]$. This is explained by the improved buoyancy condition in a higher tower, allowing the flow to better overcome friction for large enough heating zone.

10. Comparison to initial estimates

If we compare the CFD results of the simulation of the tower to the initial estimates in Section 5, we observe that the difference is considerable.

Indeed, our initial assumption have been grossly over optimistic:

1. We assumed the ground heat flux to be $1{,}361 \left[\frac{W}{m^2}\right]$ times an absorptivity of 0.99. In reality, much of the solar radiation is absorbed by the glass covering such that a better estimate of the heat flux emitted by the ground is $800 \left[\frac{W}{m^2}\right]$.
2. In the initial estimation we neglected friction, which is considerable for a $\sim 1\ [km]$ high tower.
3. In our initial estimations, we assumed that the air is uniformly heated up at the base to $60°C$, while it barely reaches a maximum of $40°C$ in a relatively small region of the heating zone.
4. In our initial estimation, we assumed that the flow velocity is uniform over the section of the tower, while in the simulation we only obtain a layer of high velocity flow near the axis.

All these assumptions ultimately caused out initial estimation to miss by two orders of magnitude.

Taking all of this into consideration, it would appear that building this type of device is not economically viable, as the power output is quite small.

11. Summary and Conclusions

5. We made a simplified calculation of a Solar Updraft Tower.
6. We, then, built an accurate simulation of a Solar Updraft Tower Power Plant, using the commercial CFD code Star-CCM+ from Siemens.
7. We performed a parametric study to investigate the influence of 2 design parameters on the operation of an Energy Tower.
8. Our CFD calculations show that the power output of this device is unexpectedly (by comparison to our initial estimations) small, making the device economically non-viable.

12. Appendix – Visualization code

Heatmaps such as *Fig. 2* were generated using the following python code:

```
import numpy as np
import matplotlib.pyplot as plt


def power_output(h, t):
    # parameter values
    R_s = 287.052874
    T_0 = 293
    d = 75
    k = 1.4
    g = 9.81
    c_p = 1004
    p_0 = 101325

    return (np.pi/4) * np.sqrt(2 * R_s * t) * p_0 * pow(d, 2) \
        * pow((pow(1 - (g * h) / (c_p * t), k / (k - 1))
               - pow(1 - (g * h) / (c_p * T_0), k / (k - 1))), 1.5)


def create_heatmap(x_range, y_range):
    # Create a grid of h and T values
    h_values = np.linspace(x_range[0], x_range[1], 100)
    t_values = np.linspace(y_range[0], y_range[1], 100)
    h, t = np.meshgrid(h_values, t_values)

    # Compute the equation value for each pair of h and T
    Z = power_output(h, t) / 1e6

    # Create the heatmap plot
    plt.figure(figsize=(10, 7))
    plt.imshow(Z, extent=[x_range[0], x_range[1], y_range[0],
y_range[1]], origin='lower', aspect='auto', cmap='viridis')
    plt.colorbar(label='Power Output [MW]')
    plt.xlabel('Tower Height [m]')
    plt.ylabel('Inside Temperature [°K]')
    plt.title('Heatmap of Power Output')
    plt.show()


if __name__ == "__main__":
    # Define the ranges for h and T variables
    h_range = (350, 700)
    T_range = (313, 353)

    create_heatmap(h_range, T_range)
```

References

[1] *"Diffuser".* (2022, February 21). Retrieved from Merriam Webster: https://www.merriam-webster.com/dictionary/diffuser

[2] *China's first solar chimney plant starts operating in desert.* (2010, 12 28). Retrieved from The People's Republic of China: Gov.cn

[3] Cloete, R. (2008, July 25). "Solar tower sheds light on little-used technology". *Engineering News Online*.

[4] Cyranoski, D. (2018, March 06). "China tests giant air cleaner to combat smog". *Nature*, pp. 555 (7695): 152-153.

[5] Energy, N. (2019). *Orot Rabin Modernization Project.* Retrieved from NS Energy: https://www.nsenergybusiness.com/projects/orot-rabin-modernization-project/

[6] Grose, T. (2014, April 14). "Solar Chimneys Can Convert Hot Air to Energy, But Is Funding a Mirage?".

[7] Hartman, L. (2022, August 16). *Wind Turbines: the Bigger, the Better.* Retrieved from Office of Energy Efficiency & Renewable Energy: https://www.energy.gov/eere/articles/wind-turbines-bigger-better

[8] Ingles, R. (1976). *Australia Patent No. AU499934B.*

[9] Lucier, R. E. (1975). *Canada Patent No. CA1023564A.*

[10]Lucier, R. E. (1979). *Israel Patent No. IL50721A.*

[11]Lucier, R. E. (1981). *United States Patent No. US4275309.*

[12]Mills, D. (2004). Advances in solar thermal electricity technology. *Solar Energy*, 76 (1-3): 19-31.

[13]sbp. (2011, August 19). *Solar Chimney Manzanares.* Retrieved from sbp: https://www.sbp.de/en/#build/show/82-Solar_Chimney_Manzanares

[14]Schlaich J, S. W. (2001, June 15). Solar Chimneys. *RA Meyers (ed), Encyclopedia of Physical Science and Technology, 3rd Edition, Academic Press, London.*

[15]*Xianha: China's first solar chimney plant starts operating in desert.* (2010, 12 27). Retrieved from xinhuanet news: News.xinhuanet.com